Microstructure and chemical stability analysis of magnetic core coated with SILICA and functionalized with silane OTS

Natália Cristina Candian Lobato[a], Angela de Mello Ferreira[b,*], Peter Georg Weidler[c], Matthias Franzreb[c], Gabriela Cordeiro Silva[d], Marcelo Borges Mansur[e]

[a] *Metallurgical and Materials Engineering Department, Universidade Federal de Minas Gerais (UFMG), Brazil*
[b] *Chemistry Department, Centro Federal de Educação Tecnológica de Minas Gerais (CEFET-MG), Brazil*
[c] *Institute for Functional Interfaces, Karlsruhe Institute of Technology (KIT), Germany*
[d] *Materials Engineering Department, Centro Federal de Educação Tecnológica de Minas Gerais (CEFET-MG), Brazil*
[e] *Metallurgical and Materials Engineering Department, Universidade Federal do Rio de Janeiro (UFRJ), Brazil*

ARTICLE INFO

Keywords:
Magnetic nanoparticles
Chemical stability
OTS silane
Silica layer

ABSTRACT

Aiming to develop hydrophobic magnetic nanoparticles that are resistant to aqueous acid mediums, the synthesis, characterization, and chemical stability analysis of a magnetite/maghemite magnetic core covered with silica and functionalized with silane OTS (NANO + SILICA + OTS) were investigated. The synthesis of the magnetic core was performed by the alkaline coprecipitation method. The coat, obtained by the sol-gel method, using TEOS silane, aims to protect the magnetic core when exposed to acidic environments. The OTS silane was used as modifier for the silica surface and provides hydrophobicity to the synthesized material; as a result, such nanoparticles are capable of being dispersed in an organic liquid. The obtained results revealed that the nanoparticles have a diameter size of approximately 10 nm, a high surface area, and a superparamagnetic behavior. The coating of the nanoparticles with silica gave the iron oxide core greater protection against oxidation and attack from acid environments. And NANO + SILICA + OTS concentrations of 20 g/L and 30 g/L in the organic fluid demonstrated that iron release from the nanoparticles to the aqueous phase was lower than 0.6% of the total iron mass, even after 24-h contact in an aqueous medium with an acidity of 2 mol/L. The obtained nanoparticles are suitable for applications, even in severe acid environments.

1. Introduction

Nanometric materials, due to their size of around 10^{-9} m, have characteristics that differ from those of the same material in a micro metric scale or larger. This phenomenon occurs because the physical properties, such as optical, electrical, thermal, and magnetic properties, are strongly linked to the size of the particles and may therefore appear differently when viewed below a critical size, normally found in a na noscale [1]. Regarding magnetic nanoparticles, due to their small vo lumes and high magnetic powers, their development has demonstrated credibility in a wide range of applications, such as mineral processing [2 9] and wastewater treatment [10 12]. Within the area of mineral processing, magnetic nanoparticles have been employed in hydro metallurgical processes, such as electrowinning [3,9], adsorption [11,12], and solvent extraction [2,4 8].

However, an unavoidable problem of magnetic nanoparticles is re lated to oxidation [13]. In mineral processes, this problem is even greater, given that, in many process steps, the particles are exposed to severe and corrosive environments, which can lead to the total de composition of the material.

One example is the use of functional nanoparticles with oleic acid in solvent extraction processes [2,4,5,8]. In this application, hydrophobic magnetic nanoparticles are dispersed in the organic phase, together with the extractant (which is the active reagent responsible for the selective extraction of the metal of interest). This organic phase is placed under agitation, together with an aqueous phase containing the metal ions, in order to promote the extraction reaction and metal transfer to the organic phase. In the subsequent stage of phase disen gagement, improvement by applying magnetic nanoparticles in this process is highlighted. Instead of separating the two phases only with the aid of the gravitational field, the use of magnetic nanoparticles al lows for a magnetic field to be applied, which guarantees a faster and more efficient disengagement. Published studies have tested the use of magnetite/maghemite nanoparticles functionalized with oleic acid and

* Corresponding author.
E-mail address: angelamello@cefetmg.br (A.d.M. Ferreira).

have obtained excellent results in decreasing the time of disengagement step [2,5,8]. Lobato et al. [2], for example, reported a time of phase disengagement step of up to 5 times faster when using the system containing 30 g/L of nanoparticles in the organic phase. However, such nanoparticles are not stable when they come into contact with aqueous solutions of pH ≤ 2. In addition, nanoparticles with no type of coating or functionalization are unstable at pH ≤ 3 [14]. Hence, it was concluded that uncoated nanoparticles, or those simply functionalized with a long carbon chain compound, do not have enough chemical resistance to be applied in aqueous systems operating within high acidity ranges.

The present study sought to create a novel composition of hydrophobic magnetic nanoparticles that are resistant to acidic liquids in an attempt to overcome this type of operating limitation. For this reason, magnetic nanoparticles of magnetite/magnetite coated with silica and functionalized with OTS silane were proposed. The synthesis of the magnetic core was performed by the alkaline coprecipitation method [2,13 18], followed by surface functionalization with oleic acid [2,4,14], in order to improve the dispersion of these particles in the next step, the sol gel process. A better dispersion of the particles in the sol gel process guarantees an individualized coating, thereby preventing the formation of a coating around a particle agglomerate. The sol gel process, based on the Stöber method, consists of the hydrolysis and condensation of the tetraethylorthosilicate precursor, named TEOS $Si(OC_2H_5)_4$, in the presence of water, alcohol, and a catalyst, which in this study was ammonia [19 21]. The silica layer formed on the surface of the nanoparticles by chemical adsorption is capable of protecting the magnetic nucleus from chemical attacks and severe environments [22]. Moreover, the silanol group terminations on the surface are capable of reacting with various coupling agents through covalent bonds so as to provide the desired characteristic particles, for example, surface hydrophobization [11,21,23]. In this work, the n octadecyltrichlorosilane (OTS) was used as a coupling agent and provided the characteristic of hydrophobicity to the synthesized material. Such synthesized nanoparticles are, therefore, capable of being dispersed in an organic liquid.

In addition to the nanoparticles with the final composition (magnetic nanoparticles coated with silica and functionalized with OTS), two other samples, nanoparticles functionalized with oleic acid and nanoparticles coated with silica, were obtained throughout the synthesis and characterized for comparison purposes and to achieve a better understanding of the synthesis process. The characterization of the samples comprised chemical composition, morphology, thermal stability, and magnetic properties. In addition, the magnetic nanoparticles coated with silica and functionalized with OTS were characterized regarding their chemical stability. This was performed to evaluate whether or not such nanoparticles are more chemically stable than oleic acid functionalized nanoparticles, as reported in published studies, and especially if an organic magnetic fluid containing these dispersed nanoparticles is capable of being industrially applied, including in processes that come into contact with acidic aqueous phases, such as solvent extractions.

2. Experimental

2.1. Materials

All reagents used in this study were analytical grade: ferric chloride hexahydrate ($FeCl_3{\cdot}6H_2O$, Vetec, purity 97%), ferrous sulphate heptahydrate ($FeSO_4{\cdot}7H_2O$, Neon, purity 99%), ammonium hydroxide (NH_4OH, Neon, 28 30 wt%), oleic acid ($C_{18}H_{34}O_2$, Synth, purity 100%), tetraethyl orthosilicate TEOS ($C_8H_{20}O_4Si$, Merck, purity ≥ 99%), trichlorooctadecylsilane OTS ($C_{18}H_{37}Cl_3Si$, Aldrich Chemistry, purity ≥ 90%), sulfuric acid (H_2SO_4, Synth, purity 98%), ethyl alcohol (CH_3CH_2OH, Neon, purity 100%), and Exxsol D80 (liquid diluent which is essentially an aliphatic hydrocarbon, ExxonMobil Chemical). The water used was either distilled or Milli Q (Millipore, France), depending on the experiment.

2.2. Synthesis of the magnetic nanoparticles

To obtain magnetic magnetite nanoparticles, which consist of the magnetic core of the coated and functionalized nanoparticles, the co precipitation synthesis method, via alkaline medium, was applied [2,13 17,24]. Thus, a solution of 0.05 mol of $FeSO_4{\cdot}7H_2O$ and 0.10 mol $FeCl_3{\cdot}6H_2O$ in 300 mL of Milli Q water was heated (80 °C) and stirred (1000 rpm). When temperature was reached, 50 mL NH_4OH (28 30%) was added dropwise, and the solution was stirred for 40 min. After this period, 6.0 mL of oleic acid were added and the solution was stirred (600 rpm) for 15 min at 60 80 °C. The system was then allowed to stand until cooled. The nanoparticles were washed with ethyl alcohol with the aid of a magnet. The nanoparticles obtained in this step were named NANO + OLEIC ACID, which consists of the magnetic core composed of magnetite/maghemite and the surface functionalization with oleic acid. The functionalization with oleic acid aims to improve the dispersion of the nanoparticles, avoiding agglomeration during the coating step with silica.

For the coating of the nanoparticles with silica through the sol gel process, 0.70 g of NANO + OLEIC ACID were dispersed in 20 mL of pure ethyl alcohol by means of a probe sonicator (Branson Ultrasonics Sonifier, 25% power and 3 cycles) for 6 min. This solution was then diluted in 120 mL of pure ethyl alcohol and placed in an ultrasonic bath (Brasonic, 1210 model, frequency 47 Hz) for 10 min. The final solution was placed under mechanical stirring (600 rpm) at room temperature. Next, 40 mL of Milli Q water and 5 mL of NH_4OH were slowly added, and the solution was stirred for 15 min. In sequence, 50 μL of tetraethyl orthosilicate (TEOS), previously diluted in 20 mL of pure ethyl alcohol, was slowly added to the solution over 5 h of stirring. After this period, the nanoparticles were washed with pure ethyl alcohol with the aid of a magnet. These silica coated particles, through the precursor TEOS, were named NANO + SILICA.

Finally, a solution containing the NANO + SILICA nanoparticles, from the previous step, was dispersed in 100 mL of ethyl alcohol (ultrasonic bath for 10 min) and placed under mechanical stirring (600 rpm) at a room temperature. Next, 35 μL of trichlorooctadecylsilane (OTS) was added to the solution, and stirring (600 rpm) was continued for 18 h. After this period, the nanoparticles were washed with ethyl alcohol and stored in pure ethyl alcohol. These silica coated and OTS functionalized nanoparticles were named NANO + SILICA + OTS.

To obtain the magnetic fluid to be used in the chemical stability test, the nanoparticles NANO + SILICA + OTS dispersed in ethyl alcohol were filtrated and dispersed directly in the Exxsol D80, by means of an ultrasonic bath for 10 min at concentrations of 10, 20, or 30 g/L.

The flow diagram of the synthesis route of magnetic nanoparticles, silica coating, and OTS functionalization is represented in Fig. 1.

2.3. Characterization of magnetic nanoparticles

The magnetic nanoparticles were characterized using the following methods:

(i) Transmission electron microscopy (TEM) analyses were performed using a Tecnai G2 20 equipment, SuperTwin FEI (200 kV). Sample preparation consisted of the dispersion of the particles in ethyl alcohol for 10 min in an ultrasonic bath, followed by dripping the sample on a carbon grid. The TEM images were analyzed for morphology and particle size information. The values of the diameters were measured using the Image J software [https://imagej.net/Welcome];

(ii) The surface area of the nanoparticles was determined by the BET (Brunauer Emmett Teller) method through nitrogen adsorption at a temperature of 95 °C with an autogassing time of 24 h. The analysis was performed using a Quantachrome Autosorb 1 MP equipment;

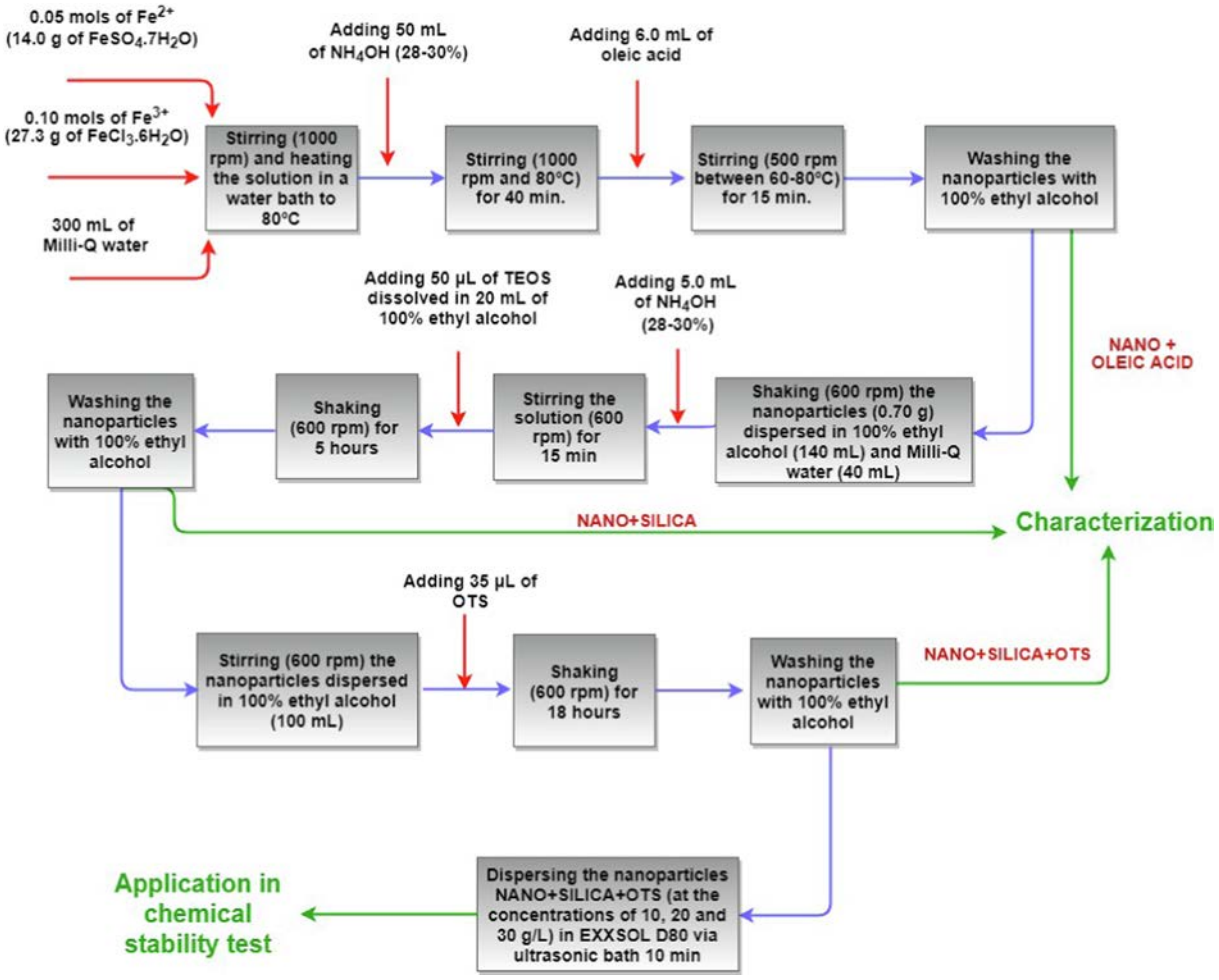

Fig. 1. Flowchart of the synthesis, coating, and functionalization process of the magnetic nanoparticles to obtain the organic magnetic fluid for application in the chemical stability test.

(iii) X ray diffraction (XRD) was used to evaluate the crystallography and the phases of the nanoparticles. The equipment used was a Bruker D8 Advance diffractometer, with a copper anode (CuKα radiation). Analyses were run with a scan range of °2θ from 15 to 80, with increments of 0.024 °2θ and a total count time of 1162 s per step. Sample preparation was performed on a sample port with the aid of a magnet below it to magnetically accumulate the particles, thereby increasing the diffraction intensity. The data were evaluated with the Bruker programs: DIFFRACT.EVA V4 and TOPAS 5.0 for the refinement of the structure [Bruker AXS (2008): TOPAS V4: General profile and structure analysis soft ware for powder diffraction data (User's Manual, Bruker AXS, Karlsruhe, Germany)]. In the Rietveld refinement [25], the fun damental parameters addressed were applied in such a way that the instrument was simulated by corresponding functions [26]. The crystal structure of the model was obtained from the Amer ican Mineralogical Society website [http://rruff.geo.arizona.edu/ AMS/amcsd.php]. The network parameters, line shapes, back ground, and fractional coordinates, according to the spatial group applied in this study (#227 Fd 3 m), were refined;

(iv) Raman spectroscopy was performed with a Jobin Yvon Horiba LABRAM HR800 spectrometer, equipped with a He Ne laser of 632.8 nm, coupled to an Olympus BX 41 microscope. The spectra were acquired with a laser power 0.08 mW and frequency range of 100 3020 cm^{-1}. The acquisition time was 60 s, with a number of samples equal to 10. This technique aimed to differentiate iron oxide phases, such as magnetite and maghemite;

(v) The Mössbauer spectroscopy analysis had the objective of con firming the composition in relation to the iron oxides of the synthesized samples. For this, the samples were analyzed using equipment with transmission mode with constant acceleration and source of 20 mCi 57Co/Rh, at room temperature (298 K). The data were numerically adjusted by Lorentzian functions with the least squares procedure of the NORMOS™ program (Brand RA, Laboratorium für Angewandte Physik, Universität Duisburg, D 47048, Duisburg, Germany). The displacement values of the iso mers were reported for α Fe at room temperature (RT);

(vi) Fourier transform infrared spectroscopy (FTIR) was carried out in a Bruker Tensor 27 infrared spectrophotometer, with the reading of the transmittance between 4000 and 450 cm^{-1}. This char acterization identified chemical groups of the bare nanoparticles, as well as the functional groups of the coating agent, in order to confirm the adsorption process;

(vii) Thermogravimetric analysis (TGA) was used to evaluate the thermal stability of the magnetic nanoparticles. The analyses were performed with the Mettler Toledo equipment. The proce dure was carried out under a nitrogen atmosphere at a flow rate of 20 mL/min and between 30 °C and 800 °C, with a heating rate of 10 °C/min;

(viii) The magnetic analyses, to obtain the magnetic behavior of the nanoparticles, were performed using the equipment Vibrating Sample Magnetometer (VSM), Lakeshore model 7404 series.

(ix) The chemical stability of the nanoparticles NANO + SILICA + OTS was determined by contacting them with

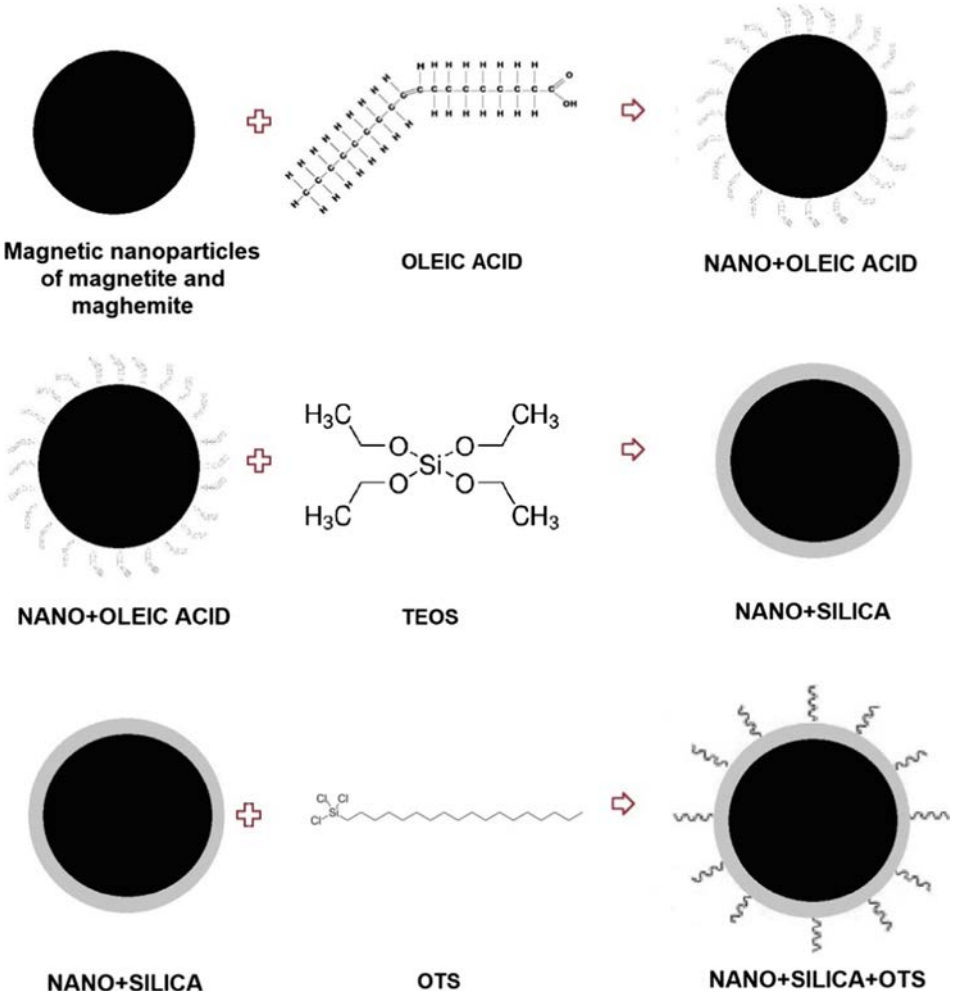

Fig. 2. Scheme of the synthesized magnetic nanoparticles.

water at changing acidity. As such nanoparticles are hydrophobic, different concentrations of the organic magnetic fluid were ob tained in order to apply them to this test. Thus, the NANO + SILICA + OTS nanoparticles were dispersed directly in Exxsol D80, by means of an ultrasonic bath for 10 min at con centrations of 10, 20, or 30 g/L. Next, 10 mL of the magnetic fluid was placed in contact with 10 mL of Milli Q water at changing acidity ($[H^+] = 10^{-7}, 10^{-6}, 10^{-5}, 10^{-4}, 10^{-3}, 10^{-2}, 10^{-1}$, 0.5, 1, and 2 mol/L). The samples were stirred in a shaker (Edmund Bühler, KL2) at 400 rpm, for 24 h, at room temperature (25 °C). Subsequently, the phases were separated, and the aqueous phase was analyzed by atomic absorption spectrophotometry (GBC, XplorAA 2 model). Thus, it was possible to evaluate how much the aqueous phase in a determined acidity was contaminated by the iron from the magnetic fluid. Such tests were performed in triplicate.

3. Results and discussion

Three different nanoparticles were collected for analysis throughout the entire synthesis process. The first is the nanoparticle functionalized with oleic acid soon after the magnetite synthesis process, named NANO + OLEIC ACID. Such a coating was performed in order to keep the nanoparticles dispersed, thus avoiding their aggregation, mainly in the sol gel coating step. The functionalization with oleic acid aims to improve the dispersion of the nanoparticles, avoiding agglomeration during the coating step with silica. When the silica coating is performed directly on the iron oxide surface, it was noticed that the size of some particles become micrometric. Consequently, these nanoparticles are not easily dispersed in the organic liquid and end up precipitate. Including, they invading the aqueous phase, when the organic solution with the nanoparticles is in contact with the surface of an aqueous solution, even though they are hydrophobic particles. This is because the repulsive force due to hydrophobicity is lower than the particle weight. So, it is important that, during the sol gel process, the nano particles be as dispersed as possible so that the silica layer is formed around each particle individually rather than around an agglomeration of particles, which could result in final particles of non nanometric size, unable to be dispersed in the fluid.

The NANO + OLEIC ACID nanoparticles were then coated with a silica layer, using the TEOS compound as a precursor in the sol gel process. This coating occurs along the entire surface of the nano particles, and its main objective is to protect them from the external environment in which the nanoparticles can be exposed, such as an acid solution. Such particles were named NANO + SILICA. Finally, to obtain hydrophobic nanoparticles, the NANO + SILICA nanoparticles were functionalized with the OTS silane, forming the NANO + SILICA + OTS nanoparticles. A scheme of coated and func tionalized nanoparticles can be seen in Fig. 2.

Transmission electron microscopy (TEM) analysis was performed on all samples to evaluate the morphology and size distribution of the nanoparticles. In the images of the NANO + OLEIC ACID (A and B), NANO + SILICA (C and D), and NANO + SILICA + OTS (E and F) shown in Fig. 3, it can be verified that samples have particle sizes

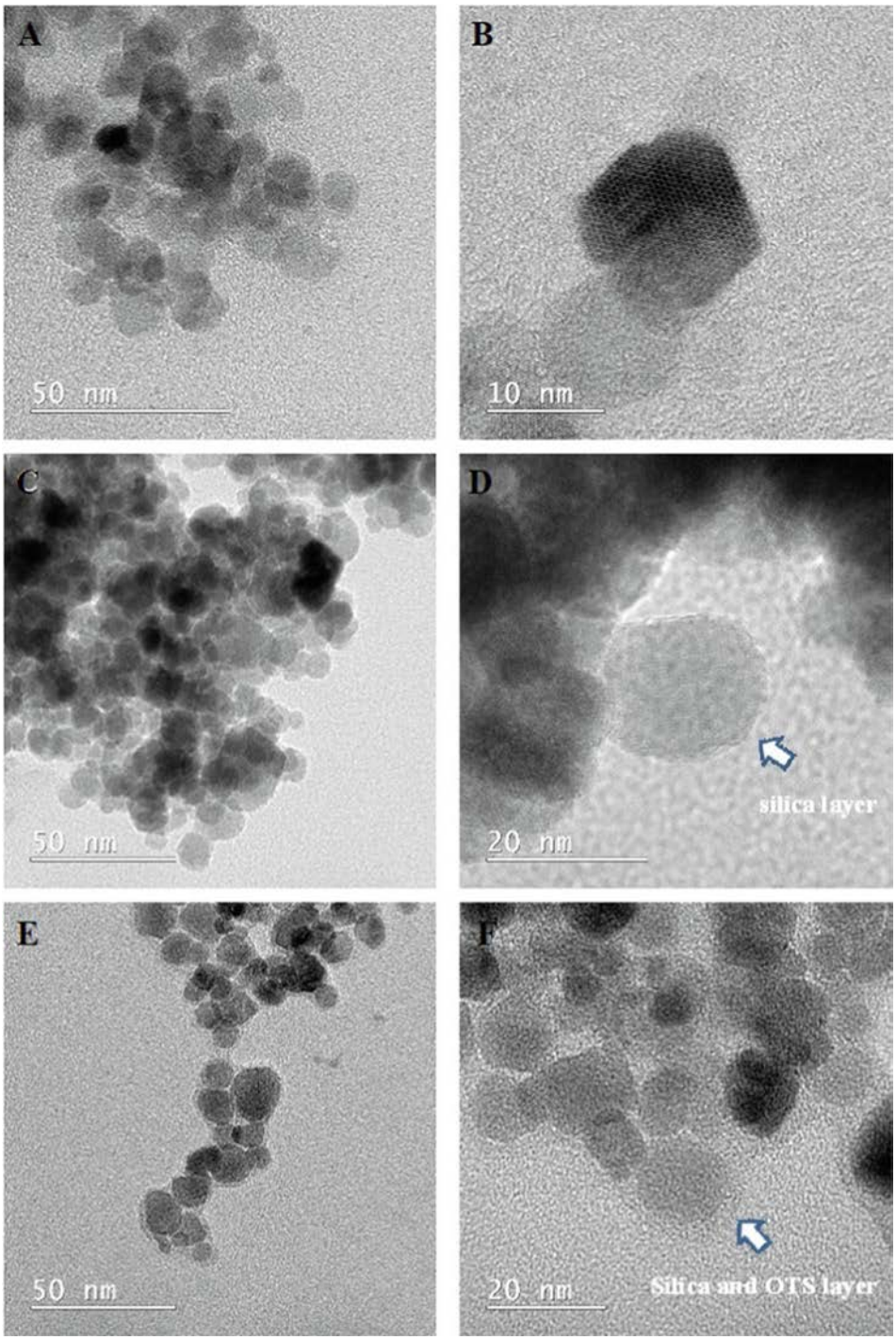

Fig. 3. Transmission electronic microscopy images of NANO + OLEIC ACID (A and B), NANO + SILICA (C and D), and NANO + SILICA + OTS (E and F).

between 10 and 20 nm, along with a homogeneous size distribution. It should be emphasized that the morphology presented no relevant var iations with the coating and particle functionalization. Moreover, in Fig. 3D, it is possible to observe the presence of the silica layer around the particles, while in Fig. 3F, the silica layer can be seen together with its functionalization with the OTS compound, which illustrates that the coating and functionalization processes were successfully completed.

For a better analysis of the size distribution, 350 particles of each sample were measured using the Image J software. The mean diameters of NANO + OLEIC ACID, NANO + SILICA, and NANO + SILICA + OTS are, respectively, 9.7, 10.4, and 10.4 nm. The histograms of the size distribution of each sample, along with the distribution profile, are shown in Fig. 4. The distribution profile follows the log normal function, as predicted in previous works [14,27].

The surface area was determined by the nitrogen adsorption tech nique and calculated by the BET method. The values found were 52.6, 78.9, and 59.2 m^2/g for the NANO + OLEIC ACID, NANO + SILICA, and NANO + SILICA + OTS samples, respectively. It was observed that the nanoparticles that have a long carbon chain adsorbed on their surfaces (NANO + OLEIC ACID and NANO + SILICA + OTS) have a smaller surface area than the particles that do not have such a char acteristic (NANO + SILICA). The same phenomenon was observed with the nanoparticles reported in previous studies [2,14], in which the nanoparticles functionalized with oleic acid (55.3 m^2/g) had a smaller

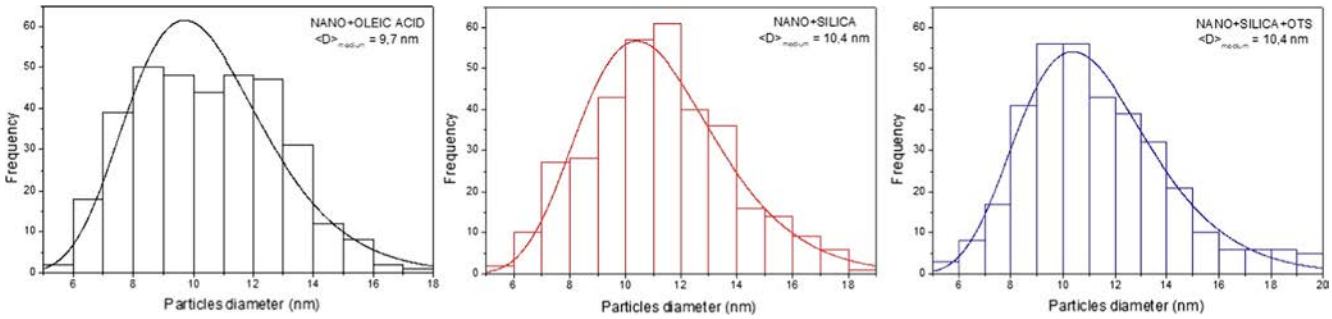

Fig. 4. Size distribution histogram of the samples: NANO + OLEIC ACID, NANO + SILICA, and NANO + SILICA + OTS.

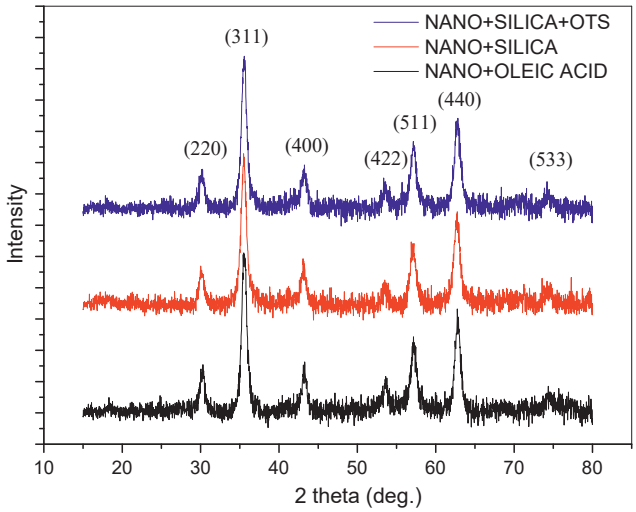

Fig. 5. X-ray diffractograms of the samples: NANO + OLEIC ACID, NANO + SILICA, and NANO + SILICA + OTS.

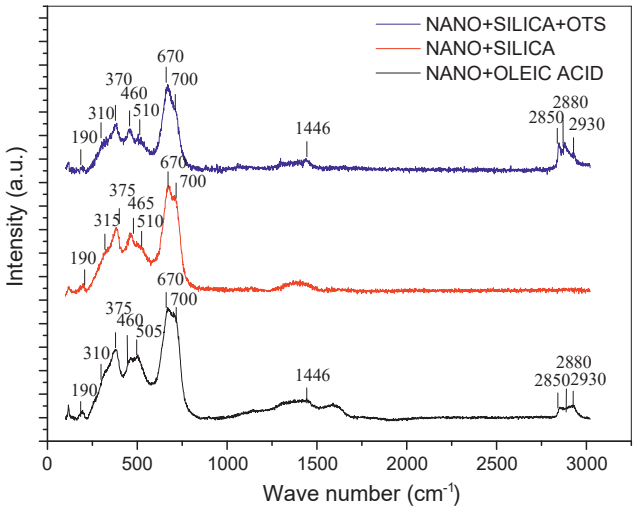

Fig. 7. Raman spectrum of the samples: NANO + OLEIC ACID, NANO + SILICA, and NANO + SILICA + OTS.

surface area when compared to nanoparticles without coating or functionalization (71.6 m^2/g) [14]. The reduction on the surface area occurs because the presence of the long carbon chains absorbed on the surface of the nanoparticles increase the particle size, which conse quently decreases the surface area of the material. The surface area of the nanoparticles coated with silica is also larger than those of the uncoated nanoparticles due to the porosity of the silica layer [2,14,28]. In this sense, the surface area of the nanoparticles NANO + SILICA + OTS is also influenced by the physical obstruction of porosity caused by the presence of the long carbon chain layer ab sorbed on the surface, which directly entails the reduction of the surface area calculated by the BET method.

The inverse spinel crystal structure, characteristic of a magnetite phase, was revealed through the identified peaks (1 1 1), (2 2 0), (3 1 1), (4 0 0), (4 2 2), (5 1 1), (4 4 0), (6 2 0), and (5 3 3) present in X ray diffractograms (Fig. 5). The diffractogram of the functionalized

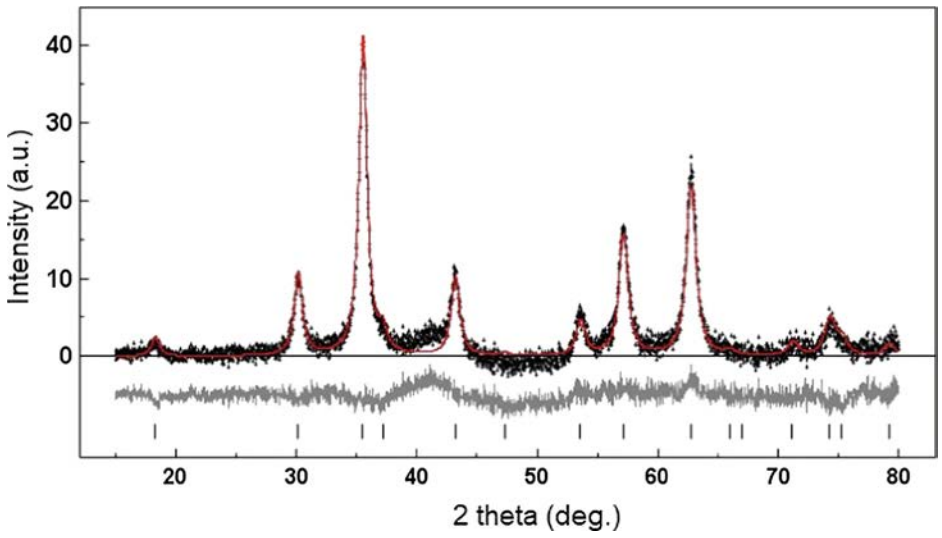

Fig. 6. Rietveld refining of the NANO + OLIC ACID sample.

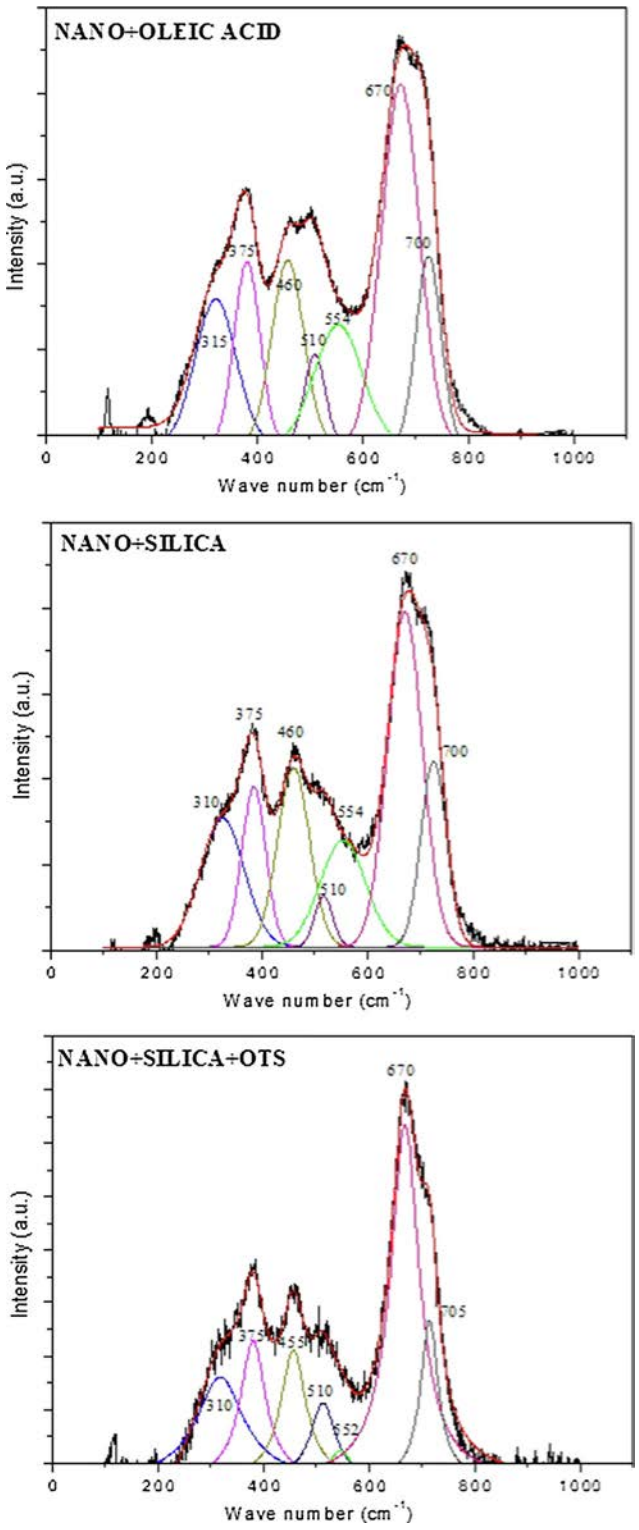

Fig. 8. Analysis of the iron oxide peaks in the samples using the PeakFit function of the Origin software.

sample with oleic acid (NANO + OLEIC ACID) was similar to the dif fractogram of the sample of nanoparticles coated with silica (NANO + SILICA), which was also similar to the sample of nano particles coated with silica and functionalized with OTS (NANO + SI LICA + OTS). Hence, it was observed that the crystalline structure remained unchanged even after the coating process, followed or not by silane functionalization, and that the crystalline portion of the samples

Table 1
Typical Raman wave number values for binding types present in nanoparticles.

Chemical compound/Chemical bonding	Wave number (cm ^{1})	References
Fe_3O_4 - T_{2g}	190–193	[36–38]
Fe_3O_4 - E_g	306–310	
γ-Fe_2O_3 - T_{2g}	350–365	
Fe_3O_4 - T_{2g}	450–490	
γ-Fe_2O_3 - E_g	500–511	
Fe_3O_4 - T_{2g}	538–554	
Fe_3O_4 - A_{1g}	668–672	
γ-Fe_2O_3 – A_{1g}	~700	
$\delta[CH_2]$	~1446	[34]
$\nu_s[CH_2]$	~2850	[35]
$\nu_a[CH_2]$	~2880	
$\nu_s[CH_3]$	~2928	

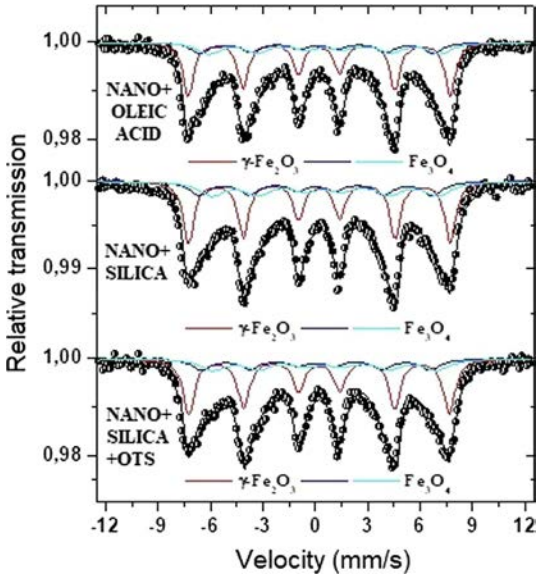

Fig. 9. Mössbauer spectra of the samples: NANO + OLEIC ACID, NANO + SILICA, and NANO + SILICA + OTS.

is comprised only of the iron oxides mentioned above, since, as ex pected, the silica layer does not form a crystalline atomic structure.

The particle size was estimated by the Scherrer equation, using the peak (3 1 1) with 2θ ~ 35.6° of the samples and considering the in strumental contribution to the line broadening [17,29,30]. It was ob served that the intensity and width of the peaks were almost identical for all samples; therefore, all estimated grain sizes of the nanoparticles were about 11.0 nm (NANO + OLEIC ACID = 11.0 nm, NANO + SI LICA = 11.1 nm, and NANO + SILICA + OTS = 11.0 nm). The nearly identical size was expected, since the crystalline iron oxide core of the three samples comes from the same synthesis and is therefore the same.

The X ray diffractograms were refined by the Pawley Fit method [31], and the network parameters of the samples were calculated, ob taining a very similar result between the samples: NANO + OLEIC ACID = 0.8372 ± 0.0002 nm, NANO + SILICA = 0.8378 ± 0.0003 nm, and NANO + SILICA + OTS = 0.8372 ± 0.0002 nm. Thus, a detailed refinement of the structure by the Rietveld method was done only for NANO + OLEIC ACID nanoparticles (see Fig. 6).

The adjustment through Rietvield refinement presented a GOF (goodness of fit) of 1.27 and a Durbin Watson Rwp parameter of 1.33. The lattice parameter was refined to 0.8372 ± 0.0001 nm. The size of the calculated magnetite domain was 9 ± 1 nm, which is consistent with the expected values, considering the size of the nanoparticles calculated by the Scherrer method, as well as the size measured by TEM. Applying the Vegard rule [32] to determine the oxidation state of magnetite, that is, by exploring a linear relationship between magnetite

Table 2
Mössbauer spectroscopy parameters of the samples NANO + OLEIC ACID, NANO + SILICA, and NANO + SILICA + OTS at room temperature.

Sample	Phases	δ (mm/s) (± 0.05)	Δ/2ξq (mm/s) (± 0.05)	B_{HF} (T) (± 0.2)	Area (%) (± 1)
NANO + OLEIC ACID (298 K)	γ-Fe_2O_3	0.31	0.01	46.5	38
	Fe_3O_4 (Fe^3) (tetrahedral site)	0.22	0.01	41.4	23
	Fe_3O_4 (Fe^3 + Fe^2) (octahedral site)	0.60	0.01	41.0	39
NANO + SILICA (298 K)	γ-Fe_2O_3	0.32	0.01	46.4	33
	Fe_3O_4 (Fe^3) (tetrahedral site)	0.22	0.01	41.4	25
	Fe_3O_4 (Fe^3 + Fe^2) (octahedral site)	0.60	0.01	44.2	42
NANO + SILICA + OTS (298 K)	γ-Fe_2O_3	0.31	0.01	46.2	39
	Fe_3O_4 (Fe^3) (tetrahedral site)	0.25	0.01	40.6	23
	Fe_3O_4 (Fe^3 + Fe^2) (octahedral site)	0.60	0.01	39.7	38

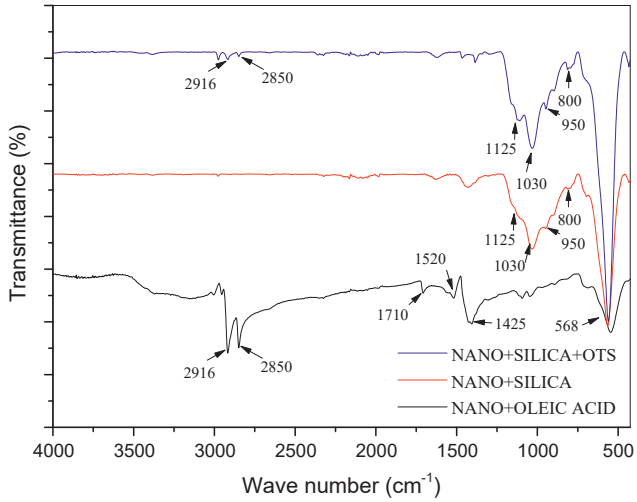

Fig. 10. FTIR spectra of the samples: NANO + OLEIC ACID, NANO + SILICA, and NANO + SILICA + OTS.

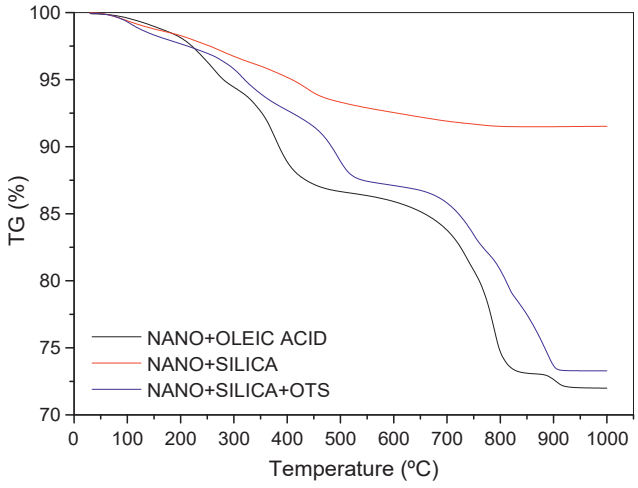

Fig. 11. Thermograms of the samples: NANO + OLEIC ACID, NANO + SILICA, and NANO + SILICA + OTS.

Table 3
Typical FTIR wave number values for binding types present in nanoparticles.

Chemical bonding	Wave number (cm ^{1})	References
ν_s[Si O Fe]	~460	[41]
ν[Fe O]	~580	[15,24,28]
ν_s[Si O Si]	790–800	[34,41]
ν[Si OH]	950	[34,41]
ν_{as}[Si O Si]	1030–1050 e 1120–1150	[28,34]
ν_s[COO]	1404–1425	[15,39]
ν_{as}[COO]	1520–1530	[15,39]
$C_{18}H_{34}O_2$ (free oleic acid)	1700–1750	[39,40]
ν_s [C H]	2850	[15,24,34]
ν_{as}[C H]	~2920	[15,24,34]

and maghemite network parameters and its oxidation state, a degree of oxidation of 36% can be deduced based on the variation of the net parameter of the refined sample, which resulted in the chemical for mula $Fe_{2.88}\square_{0.12}O_4$, which □ indicates vacancy. Whereas the general formula for non oxidized magnetite is Fe_3O_4, for maghemite is $Fe_{2.66}\square_{0.33}O_4$, and for oxidized magnetite is $Fe_{3\ x}\square_xO_4$, it can therefore be concluded that the degree of oxidation of the sample is low but significant.

The Raman analysis was performed between 100 and 3020 cm^{-1} in order to confirm the presence of the magnetite and maghemite phases in the samples, as well as the presence of the carbonic chain characteristics of oleic acid and OTS (n octadecyl trichlorosilane). All obtained spectra showed the characteristic peaks of magnetite and maghemite (see Fig. 7). Peaks 190, 310, 460, and 679 cm^{-1} are mag netite peaks, while peaks 370, 510, and 700 cm^{-1} are characteristic of the maghemite phase. To better evaluate the presence of these two phases in the sample, peaks were adjusted between 100 and 1000 cm^{-1}, using the PeakFit function from the Origin program (see Fig. 8). With the adjustment made, the presence of all characteristic peaks of the samples was observed, including the peak of approximately 550 cm^{-1} regarding magnetite. Thus, it can be concluded that both phases are present in the samples.

Moreover, all of the spectra of the samples in Fig. 7 show a broad peak around 1300 1500 cm^{-1}. According to El Mendili et al. [33], the occurrence of this broad peak (magnon mode) is linked to the char acteristic of the antiferromagnetic structure of maghemite. However, the NANO + OLEIC ACID and NANO + SILICA + OTS samples present a more prominent peak in this region (~1446 cm^{-1}) relative to the CH_2 bond. This binding is characteristic of oleic acid and n octadecyl tri chlorosilane (OTS) compounds, which have a carbon chain of 18 car bons each [34]. The samples NANO + OLEIC ACID and NANO + SI LICA + OTS also show peaks of 2850, 2880, and 2930 cm^{-1}, referring, respectively, to the asymmetric and symmetric vibration of CH_2 and the symmetric vibration of CH_3 [35]. The relationship between the con nection types and the corresponding wave number is summarized in Table 1.

The occurrence of magnetite and maghemite was also identified by

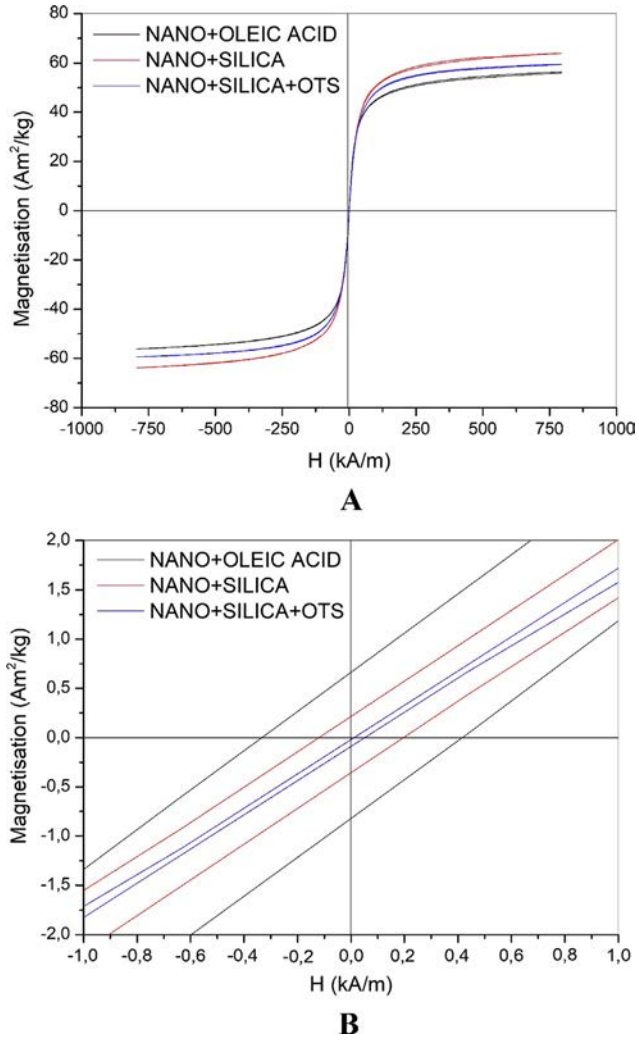

Fig. 12. Hysteresis curves (A) and coercivity field values (B) of the samples: NANO + OLEIC ACID, NANO + SILICA, and NANO + SILICA + OTS.

Table 4
Saturation magnetization, and coercivity values of the magnetic nanoparticles.

Sample	Coercivity H_c (kA/m)	Magnetization M_s (Am^2/kg)
NANO + OLEIC ACID	0.37	52
NANO + SILICA	0.15	59
NANO + SILICA + OTS	0.02	56

Mössbauer spectroscopy analysis. The spectrum obtained for the samples at 298 K (Fig. 9) shows six broad lines. The broad line patterns can be attributed to the finite size effect and/or the spin relaxation of the analyzed nanoparticles, in addition to suggesting a superparamagnetic behavior of the samples at room temperature. Through the use of NORMOS™ software, the spectra were adjusted with three different sextets referring to the phases of magnetite and maghemite. The hyperfine parameters obtained by the analysis are presented in Table 2. These parameters (δ, Δ/2ξq, and BHF) showed no significant changes among the samples, indicating that the coating and/or functionalization did not alter the hyperfine structures of magnetite or maghemite. The results show that NANO + OLEIC ACID nanoparticles have a composition of 38% maghemite and 62% magnetite, whereas NANO + SILICA particles are composed of 33% maghemite and 67% magnetite and NANO + SILICA + OTS, 39% maghemite and 61% magnetite, in satisfactory agreement with XRD analysis.

Through infrared spectroscopy (FTIR), the functionalization and surface coating of the magnetic nanoparticles were observed. Fig. 10 shows the spectra of the samples: NANO + OLEIC ACID, NANO + SILICA, and NANO + SILICA + OTS. The three samples present the band 568 cm^{-1}, corresponding to the vibration of the Fe—O bond [15,24,28]. The sample of nanoparticles functionalized with oleic acid (NANO + OLEIC ACID) has bands at 1425 and 1520 cm^{-1}, which are attributed to the symmetric and asymmetric vibration of the carboxyl group (COO—) of the surfactant, respectively, and the bands 2850 and 2915 cm^{-1}, corresponding, respectively, to the symmetrical and asymmetric stretching modes of the CH bonds of oleic acid [15,24]. In addition, this sample also presents the band 1710 cm^{-1}, which corresponds to the free oleic acid vibration, meaning that there was an excess of this surfactant in the functionalization process [39,40]. On the other hand, the samples covered with silica or covered with silica and functionalized with OTS (NANO + SILICA and NANO + SILICA + OTS) present the band related to the iron oxygen bond around 570 cm^{-1} and, together with this, the Si O Fe band around 460 cm^{-1}. Due to the overlap between these two bands, the peak detected around 570 cm^{-1} for the samples containing silicon show a higher intensity. The interference between these bands has already been mentioned in the literature [41]. In addition, bands 1030 and 1125 cm^{-1} for Si—O—Si binding, the 950 cm^{-1} band for Si—OH binding, and the 800 cm^{-1} band corresponding to Si—O—Si binding [28,34,41]. In the sample NANO + SILICA + OTS, in addition to the aforementioned bands, the occurrence of bands at 2850 and 2915 cm^{-1}, referent to the C—H bonds, present in the long carbonic chain of the OTS compound were identified. The relationship between the connection types and the corresponding wave number is summarized in Table 3.

It was observed that the characteristic bands of oleic acid (1425 and 1520 cm^{-1}) disappear in the sample of silica coated nanoparticles. It can therefore be concluded that the bonds between the oleic acid molecules and the nanoparticles are undone during the coating process of the magnetic nanoparticles via sol gel. The bands 2850 and 2915 cm^{-1} reappear in the NANO + SILICA + OTS sample due to the OTS molecule used to make the nanoparticles hydrophobic. This silane has, much like oleic acid, an 18 carbon carbon chain and consequently has C H bonds.

Fig. 11 shows the thermograms of the three characterized samples. The NANO + OLEIC ACID sample presents four stages of decomposition. Up to the temperature of 120 °C, the weight loss refers to the evaporation of water and/or alcohol adsorbed onto the particles, about 0.6%. From 120 °C to 270 °C and from 270 °C to 450 °C, respectively, correspond to the decomposition of the oleic acid adsorbed (4.0%) and chemically adsorbed (7.6%) layers on the nanoparticle surfaces [15,40]. The last step between 450 °C and 800 °C is a loss of 15.7% by mass. As already mentioned in the characterization of oleic acid functionalized nanoparticles from the first synthesis of this work, this thermogram stage refers to the degradation of oleic acid, which produces gases, such as CO and CO_2, responsible for the reduction of magnetic nanoparticles [42]. The NANO + SILICA sample presents a weight loss of 0.9% up to 120 °C referring to the water and/or alcohol molecules on its surface. The weight loss, from 200 °C to 350 °C, of 3.1%, is due to the decomposition of non hydrolyzed ethoxy groups. Weight loss at a higher temperature (350 650 °C) is also associated with the condensation of the silanol chemistry group on the nanoparticle surfaces, forming a stable Si—O—Si layer (4.5%) [43,44]. Finally, in the NANO + SILICA + OTS sample, between room temperature and 120 °C, the weight loss consists of water and alcohol molecules on the surface of the nanoparticles (1.1%). The desorption of the physically and chemically adsorbed OTS layers appear in the following temperature ranges, respectively: 120 °C to 350 °C (5.0%) and 350 °C to 550 °C (6.2%). In these temperature ranges, the decomposition of non hydrolyzed ethoxy groups present on the silica may also occur. The final stage, between 550 °C and 800 °C, is a step in which there is still a loss of organic matter, a loss of —OH present in silica and magnetite, a decomposition of the magnetic nucleus (i.e. magnetite),

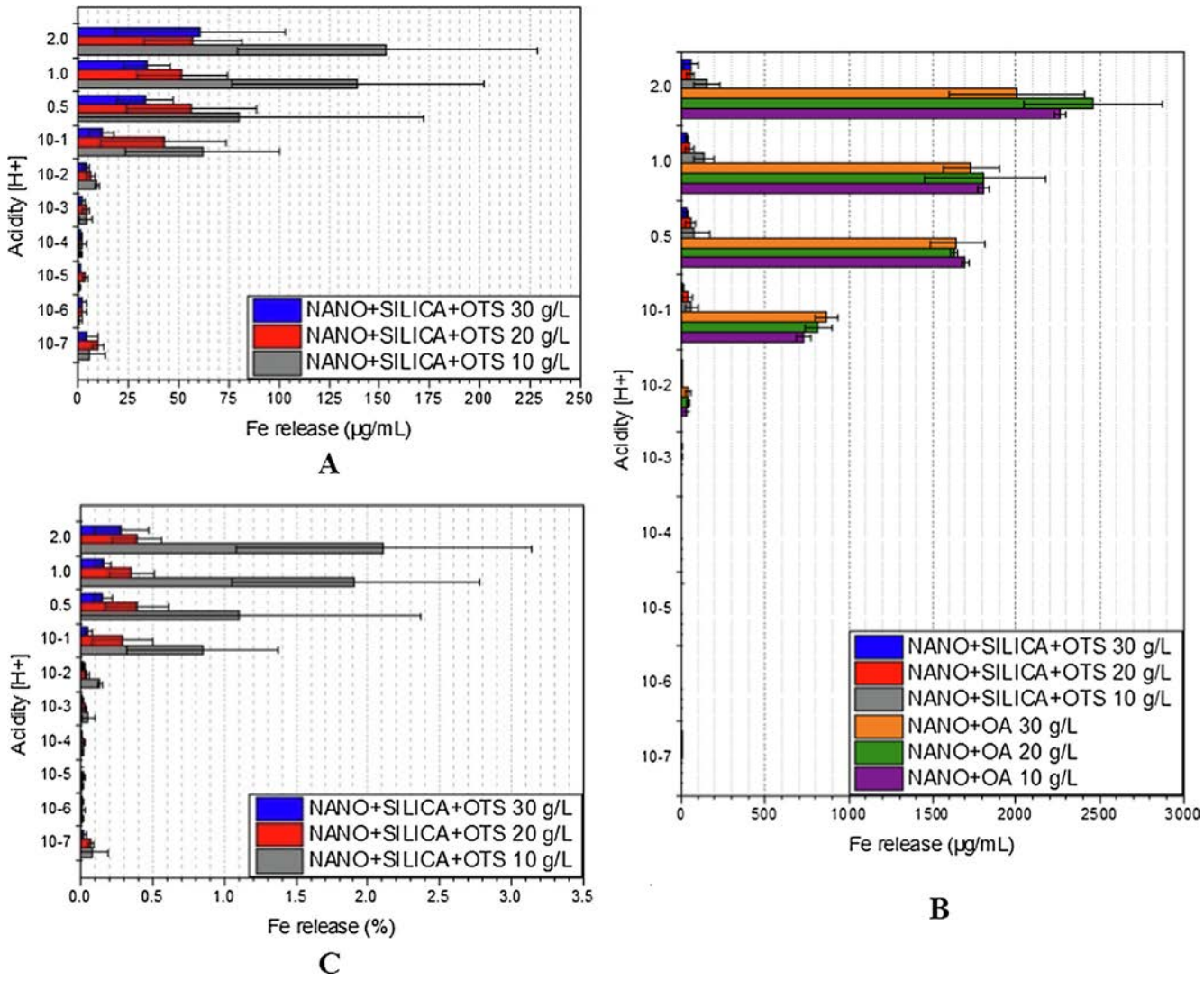

Fig. 13. Iron release from the magnetic nanoparticles NANO + SILICA + OTS (A), Iron release comparation of NANO + SILICA + OTS and NANO + OA nanoparticles (B) and percentage of iron release from the magnetic nanoparticles NANO + SILICA + OTS (C) during the chemical stability test.

and a condensation of the chemical silanol group on the surface of the nanoparticles (14.4%) [43,45]. Fig. 11 also illustrates that the amount of matter added to the surface of the nanoparticles (magnetic core) increases in the following order: NANO + SILICA, NANO + SI LICA + OTS, and NANO + OLEIC ACID.

The hysteresis curves of the magnetic nanoparticles are shown in Fig. 12 A, exhibiting the samples' magnetization values of between 52 and 59 Am2/kg. It is observed that the samples showed a small coer civity value (Fig. 12 B), leading to the conclusion that most of the particles are in the superparamagnetic state. The effect of less coercivity most likely occurs due to a better dispersion of the nanoparticles, which favors a residual nonmagnetization. The data obtained by the analysis are shown in Table 4. It is also important to note that the decrease in the saturation magnetization value is related to the percentage of nonmagnetic matter present in the nanoparticles. As previously men tioned, the amount of nonmagnetic matter present on the surface of nanoparticles increases in the following sequence: NANO + SILICA, NANO + SILICA + OTS, and NANO + OLEIC ACID. This relationship is directly related to the decreasing order of magnetization: NANO + SILICA (59 Am^2/kg), NANO + SILICA + OTS (56 Am^2/kg), and NANO + OLEIC ACID (52 Am^2/kg), reaffirming that the decrease in the magnetization value of magnet nanoparticle samples is due to the presence of nonmagnetic material, in this case, oleic acid, silica, and OTS.

To evaluate the chemical stability of nanoparticles when in contact with environments of varied acidity, the chemical stability test was performed using NANO + SILICA + OTS nanoparticles. These nano particles were dispersed in the organic liquid (Exxsol D80) in the fol lowing concentrations: 10, 20, and 30 g/L. Samples of each of these concentrations were placed in contact with aqueous solutions of varying acidities: $[H^+] = 10^{-7}, 10^{-6}, 10^{-5}, 10^{-4}, 10^{-3}, 10^{-2}, 10^{-1}$, 0.5, 1, and 2 mol/L. Here, 10 mL of each organic phase, together with 10 mL of the aqueous phase, were shaken for 24 h.

The results presented in the Fig. 13A show the iron release in the aqueous phase in µg/mL. It was observed that the presence of iron in creased in direct proportion with acidity, as expected. When comparing the results obtained in the present work with those obtained by Lobato et al. [2], which performed the same chemical stability test with na noparticles functionalized with oleic acid, it was noted that the mag netic nanoparticles coated with silica and functionalized OTS are much more resistant. Data from both systems were plotted in Fig. 13B, by which it is possible to observe the discrepancy of iron contamination between the different nanoparticle composition systems. The results reported by Lobato et al. [2] show that the nanoparticles functionalized with oleic acid (NANO + OA) present in the organic fluid at a con centration of 30 g/L and in contact with 2 mol/L aqueous solution

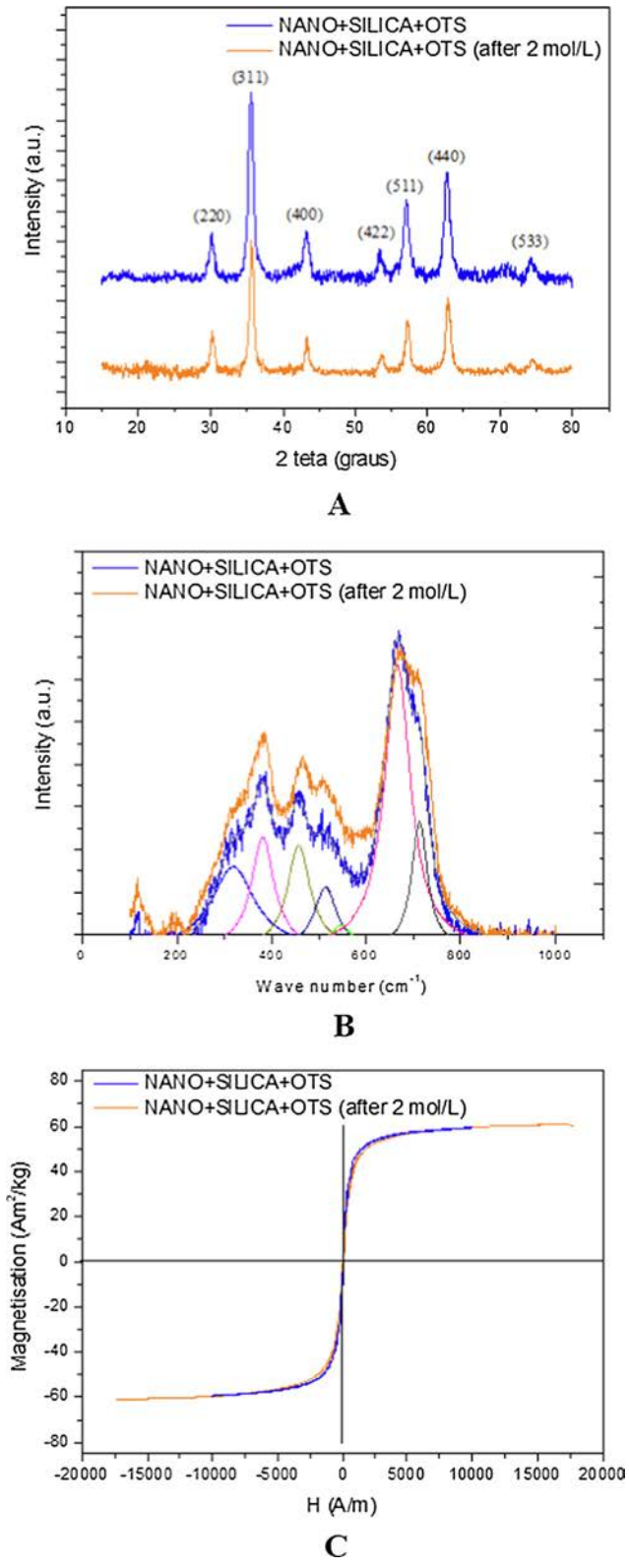

Fig. 14. X-ray diffraction (A), Raman spectroscopy (B) and magnetic analyzes (C) of the nanoparticles coated with silica and functionalized with OTS sample before (NANO + SILICA + OTS) and after the chemical stability test in an acid solution of 2 mol/L (NANO + SILICA + OTS after 2 mol/L).

release about 2000 μg/mL of iron, while the nanoparticles of this work under the same conditions only presented an iron release of 61 μg/mL, that is, NANO + SILICA + OTS nanoparticles were about 30 times more stable than nanoparticles functionalized with oleic acid. At pH = 1 and a concentration of 30 g/L, the system with nanoparticles functionalized with oleic acid contaminated the aqueous phase with 869 μg/mL of iron, whereas the system with nanoparticles coated with silica and functionalized OTS, this contamination was 12 μg/mL of iron. In this specific condition, the resistance of NANO + SILICA + OTS nanoparticles was 72 times higher. Evaluating all the results obtained, at different concentrations, NANO + SILICA + OTS nanoparticles are on average 32 times more resistant than NANO + OA nanoparticles. This higher stability is related to the greater protection that the silica layer provides to the nanoparticle cores, which consists of the magne tite and maghemite phases. With the hydrolysis and condensation re actions of TEOS that occur during the sol gel process, the silica layer (SiO_2), which forms on the surface of nanoparticles, protects the mag netic core against acidic media, chemical attacks, and severe environ ments [11,21,23,28,46,47]. The small iron release that may still occur is due to the existing silica porosity [28].

Fig. 13C shows the percentage of iron release from the organic phase with NANO + SILICA + OTS nanoparticles to the aqueous phase during the chemical stability test. Note that the higher the amount of nanoparticles present in the fluid, the lower the percentage of iron re leased in the aqueous phase, as observed in previous studies [2]. Such a behavior is related to the change in the physical properties of the fluids due to the presence of nanoparticles, such as density, surface tension, and viscosity, which can affect the immiscibility between the phases and the mobility of the particles [48,49]. That is, the more concentrated the fluid, the higher the viscosity, the higher the surface tension, and, consequently, the higher the immiscibility, which favors the chemical stability of the particles.

In fact, it can be concluded that an organic phase containing the NANO + SILICA + OTS nanoparticles with a concentration of 20 30 g/ L presents an iron release of less than 0.6% even after 24 h of contact in an aqueous medium with an acidity of equal to 2 mol/L.

In order to prove the physical and chemical stability of nano particles in contact with very acidic solutions over a long period, the NANO + SILICA + OTS nanoparticles obtained from the 2 mol/L chemical stability assay [30 g/L of nanoparticles, 24 h] were evaluated regarding their crystallography, chemical composition and magnetic behavior, through the following respectively analyzes: X ray diffraction (DRX), Raman spectroscopy and magnetic analyzes.

In Fig. 14A, the X ray diffractogram of the sample after the chemical stability test (NANO + SILICA + OTS (after 2 mol/L)) shows the same characteristic peaks of magnetite phase revealed by the nanoparticles coated with silica and functionalized with OTS sample (NANO + SI LICA + OTS). Already the Raman analysis, performed between 100 and 1000 cm^{-1}, revealed that the NANO + SILICA + OTS (after 2 mol/L) sample presents all characteristic peaks of magnetite and maghemite, presenting the same spectrum structure of the NANO + SILICA + OTS sample as can be seen in Fig. 14B. Thus, through the XRD and Raman analysis, it was concluded that the chemical and crystallographic structure of the magnetic core of the NANO + SILICA + OTS nano particles did not change after the chemical stability test in contact with 2 mol/L aqueous solution for 24 h. Finally, the magnetic behavior was evaluated through the hysteresis curve of the sample that underwent chemical attack. As can be seen in Fig. 14C, it is noted that there was no change in the saturation magnetization and the coercivity value. Thus, it is found that the nucleus remains superparamagnetic and with the same magnetic properties. It is concluded, therefore, that such analyzes prove that the silica layer actually protects the magnetic core of it, thus preventing a chemical degradation, or substantial oxidation or phase change of the iron oxide core, which can cause the formation of a nonmagnetic iron oxide phase.

Hence, it can be concluded that these nanoparticles are chemically suitable for industrial applications even in very severe environments.

4. Conclusions

During the synthesis, coating, and functionalization of nanoparticles with silanes, three samples from different points of the synthesis were obtained and characterized: nanoparticles functionalized with oleic acid (NANO + OLEIC ACID), nanoparticles coated with silica (NANO + SILICA), and nanoparticles coated with silica and functio nalized with silane OTS (NANO + TEOS + OTS). The three different samples presented an average particle diameter of around 10 nm, a high surface area (between 52.6 and 78.9 m^2/g), and a mineralogical com position of magnetite and maghemite, which is the predominant mag netite phase with more than 60%. Moreover, these samples presented a behavior that was quite close to superparamagnetism, with a low coercivity value and a high saturation magnetization value (between 52 and 59 Am^2/kg). The coating of the nanoparticles with silica gave the iron oxide core greater protection against oxidation and attack from acid environments. Hydrophobization with OTS was also efficient be cause the particles remained in the organic phase even after intense agitation between the phases. As for the chemical stability tests, these showed that, at the concentrations of the fluid containing the nano particles NANO + SILICA + OTS of 20 g/L and 30 g/L, the iron release of the nanoparticles to the aqueous phase was less than 0.6% of the total iron mass of the organic phase, even after 24 h of contact in an aqueous medium with acidity equal to 2 mol/L. Furthermore, it was proved that these hydrophobic magnetic nanoparticles that had contact with the acidic solution in the most severe condition (2 mol/L) did not change in their crystallographic structure, chemical composition and magnetic behavior, proving that the silica layer is really efficient re garding the iron oxide core protection. Thus, it can be concluded that nanoparticles coated with silica and functionalized with OTS at con centrations of 20 30 g/L are suitable for to be applied in all solvent extraction systems, including the operations of copper, cobalt, nickel and/or zinc recovery, which are systems that normally operate in one or more of the steps under highly acidic conditions (pH < 1) [50 52]. Moreover, such nanoparticles can be adapted and evaluated for appli cations as an oil collector, for example in petroleum oil spill disasters in sea or rivers [53].

Acknowledgement

The authors wish to acknowledge CNPq, CAPES PROEX, FAPEMIG, and the Erasmus Mundus Programme for their financial support; the Center of Microscopy at Universidade Federal de Minas Gerais (UFMG) (http://www.microscopia.ufmg.br) for providing the equipment and technical support for experiments involving electron microscopy; and Centro de Desenvolvimento da Tecnologia Nuclear (CDTN) (http://www.cdtn.br/) for their support with Mössbauer spectroscopy analysis.

References

[1] G. Cao, Y. Wang, Nanostructures and nanomaterials - Synthesis, properties and applications, in: World Scientific Series in Nanoscience and Nanotechnology, vol. 2, 2011, ISBN: 9789814324557.
[2] N.C.C. Lobato, A. de M. Ferreira, M.B. Mansur, Evaluation of magnetic nanoparticles coated by oleic acid applied to solvent extraction processes, Sep. Purif. Technol. 168 (2016) 93–100, https://doi.org/10.1016/j.seppur.2016.05.027.
[3] U. Condomitti, A. Zuin, A.T. Silveira, K. Araki, H.E. Toma, Magnetic nanohydrometallurgy: a promising nanotechnological approach for metal production and recovery using functionalized superparamagnetic nanoparticles, Hydrometallurgy 125–126 (2012) 148–151, https://doi.org/10.1016/j.hydromet.2012.06.005.
[4] J.Y. Hwang, Magnetic solvent extraction, 5,043,070, 1991.
[5] L.L. Vatta, K.R. Koch, K.C. Sole, The potential use of hydrocarbon magnetic liquids in solvent extraction, in: Proc. ISEC - Int. Solvent Extr. Conf., 2008, p. 1513–1518. doi: 1-894475-80-1.
[6] Q. Wang, Y. Guan, X. Ren, G. Cha, M. Yang, Rapid extraction of low concentration heavy metal ions by magnetic fluids in high gradient magnetic separator, Sep. Purif. Technol. 82 (2011) 185–189, https://doi.org/10.1016/j.seppur.2011.09.011.
[7] Q. Wang, Y. Guan, X. Ren, M. Yang, X. Liu, Application of magnetic extractant for the removal of hexavalent chromium from aqueous solution in high gradient magnetic separator, Chem. Eng. J. 183 (2012) 339–348, https://doi.org/10.1016/j.cej.2012.01.005.
[8] W. Palyska, A.G. Chmielewski, Solvent extraction and emulsion separation in magnetic fields, Sep. Sci. Technol. 28 (1993) 127–138.
[9] H.E. Toma, Developing nanotechnological strategies for green industrial processes, Pure Appl. Chem. 85 (2013) 1655–1669, https://doi.org/10.1351/PAC-CON-12-12-02.
[10] A. Drenkova-Tuhtan, K. Mandel, A. Paulus, C. Meyer, F. Hutter, C. Gellermann, G. Sextl, M. Franzreb, H. Steinmetz, Phosphate recovery from wastewater using engineered superparamagnetic particles modified with layered double hydroxide ion exchangers, Water Res. 47 (2013) 5670–5677, https://doi.org/10.1016/j.watres.2013.06.039.
[11] F. Ge, M.-M. Li, H. Ye, B.-X. Zhao, Effective removal of heavy metal ions Cd^{2+}, Zn^{2+}, Pb^{2+}, Cu^{2+} from aqueous solution by polymer-modified magnetic nanoparticles, J. Hazard. Mater. 211–212 (2012) 366–372, https://doi.org/10.1016/j.jhazmat.2011.12.013.
[12] G.C. Silva, F.S. Almeida, A.M. Ferreira, V.S.T. Ciminelli, Preparation and application of a magnetic composite (Mn_3O_4/Fe_3O_4) for removal of As(III) from aqueous solutions, Mater. Res. 15 (2012) 403–408, https://doi.org/10.1590/S1516-14392012005000041.
[13] R.M. Cornell, U. Schwertmann, The Iron Oxides: Structure, Properties, Reactions, Occurrences and Uses, Wiley-VCH, Weinheim, 2003 doi:10.1002/3527602097.
[14] N.C.C. Lobato, M.B. Mansur, A. de M. Ferreira, Characterization and chemical stability of hydrophilic and hydrophobic magnetic nanoparticles, Mater. Res. 20 (2017) 736–746, https://doi.org/10.1590/1980-5373-mr-2016-0707.
[15] K. Petcharoen, A. Sirivat, Synthesis and characterization of magnetite nanoparticles via the chemical co-precipitation method, Mater. Sci. Eng. B Solid-State Mater. Adv. Technol. 177 (2012) 421–427, https://doi.org/10.1016/j.mseb.2012.01.003.
[16] M.T. López-López, J.D.G. Durán, A.V. Delgado, F. González-Caballero, Stability and magnetic characterization of oleate-covered magnetite ferrofluids in different nonpolar carriers, J. Colloid Interface Sci. 291 (2005) 144–151, https://doi.org/10.1016/j.jcis.2005.04.099.
[17] V. Lobaz, R.N.K. Taylor, W. Peukert, Highly magnetizable superparamagnetic colloidal aggregates with narrowed size distribution from ferrofluid emulsion, J. Colloid Interface Sci. 374 (2012) 102–110, https://doi.org/10.1016/j.jcis.2012.01.057.
[18] M.C. Bagatini, V. Zymla, E. Osório, A.C.F. Vilela, Characterization and reduction behavior of mill scale, ISIJ Int. 51 (2011) 1072–1079, https://doi.org/10.2355/isijinternational.51.1072.
[19] W. Stöber, A. Fink, E. Bohn, Controlled growth of monodisperse silica spheres in the micron size range, J. Colloid Interface Sci. 26 (1968) 62–69, https://doi.org/10.1016/0021-9797(68)90272-5.
[20] P.I. Girginova, A.L. Daniel-da-Silva, C.B. Lopes, P. Figueira, M. Otero, V.S. Amaral, E. Pereira, T. Trindade, Silica coated magnetite particles for magnetic removal of Hg^{2+} from water, J. Colloid Interface Sci. 345 (2010) 234–240, https://doi.org/10.1016/j.jcis.2010.01.087.
[21] S.H. Im, T. Herricks, Y.T. Lee, Y. Xia, Synthesis and characterization of monodisperse silica colloids loaded with superparamagnetic iron oxide nanoparticles, Chem. Phys. Lett. 401 (2005) 19–23, https://doi.org/10.1016/j.cplett.2004.11.028.
[22] E. Tahmasebi, Y. Yamini, Facile synthesis of new nano sorbent for magnetic solid-phase extraction by self assembling of bis-(2,4,4-trimethyl pentyl)-dithiophosphinic acid on Fe_3O_4@Ag core@shell nanoparticles: characterization and application, Anal. Chim. Acta. 756 (2012) 13–22, https://doi.org/10.1016/j.aca.2012.10.040.
[23] Y.-H. Deng, C.-C. Wang, J.-H. Hu, W.-L. Yang, S.-K. Fu, Investigation of formation of silica-coated magnetite nanoparticles via sol–gel approach, Colloids Surf. A Physicochem. Eng. Asp. 262 (2005) 87–93, https://doi.org/10.1016/j.colsurfa.2005.04.009.
[24] M.R. Mauricio, H.R. de Barros, M.R. Guilherme, E. Radovanovic, A.F. Rubira, G.M. de Carvalho, Synthesis of highly hydrophilic magnetic nanoparticles of Fe_3O_4 for potential use in biologic systems, Colloids Surf. A – Physicochem. Eng. Asp. 417 (2013) 224–229, https://doi.org/10.1016/j.colsurfa.2012.11.014.
[25] H.M. Rietveld, Line profiles of neutron powder-diffraction peaks for structure refinement, Acta Crystallogr. 22 (1967) 151–152, https://doi.org/10.1107/S0365110X67000234.
[26] R.W. Cheary, A. Coelho, A fundamental parameters approach to X-ray line-profile fitting, J. Appl. Crystallogr. 25 (1992) 109–121, https://doi.org/10.1107/S0021889891010804.
[27] L.B. Kiss, J. Söderlund, G.A. Niklasson, C.G. Granqvist, New approach to the origin of lognormal size distributions of nanoparticles, Nanotechnology 10 (1999) 25–28, https://doi.org/10.1088/0957-4484/10/1/006.
[28] M. Kuzminska, N. Carlier, R. Backov, E.M. Gaigneaux, Magnetic nanoparticles: improving chemical stability via silica coating and organic grafting with silanes for acidic media catalytic reactions, Appl. Catal. A Gen. 505 (2015) 200–212, https://doi.org/10.1016/j.apcata.2015.08.005.
[29] O.M. Lemine, K. Omri, M. Iglesias, V. Velasco, P. Crespo, P. de la Presa, L. El Mir, H. Bouzid, A. Yousif, A. Al-Hajry, γ-Fe_2O_3 by sol–gel with large nanoparticles size for magnetic hyperthermia application, J. Alloys Compd. 607 (2014) 125–131, https://doi.org/10.1016/j.jallcom.2014.04.002.
[30] P. Scherrer, Bestimmung der Größe und der inneren Struktur von Kolloidteilchen mittels Röntgenstrahlen, Nachrichten von der Gesellschaft der Wissenschaften zu Göttingen, Math. Klasse. 26 (1918) 98–100 https://eudml.org/doc/59018#.WcBx6t9OCXs.mendeley.
[31] G.S. Pawley, Unit-cell refinement from powder diffraction scans, J. Appl. Crystallogr. 14 (1981) 357–361, https://doi.org/10.1107/S0021889881009618.
[32] L. Vegard, Die Konstitution der Mischkristalle und die Raumfullung der Atome, Zeitschrift fur Phys. 5 (1921) 17–26, https://doi.org/10.1007/BF01349680.

[33] Y. El Mendili, J.-F. Bardeau, N. Randrianantoandro, A. Gourbil, J.-M. Greneche, A.-M. Mercier, F. Grasset, New evidences of in situ laser irradiation effects on γ-Fe2O3 nanoparticles: a Raman spectroscopic study, J. Raman Spectrosc. 42 (2011) 239–242, https://doi.org/10.1002/jrs.2762.
[34] Y.-S. Li, J.S. Church, A.L. Woodhead, F. Moussa, Preparation and characterization of silica coated iron oxide magnetic nano-particles, Spectrochim. Acta Part A Mol. Biomol. Spectrosc. 76 (2010) 484–489, https://doi.org/10.1016/j.saa.2010.04.004.
[35] Z. Liao, C.J. Orendorff, L.C. Sander, J.E. Pemberton, Structure function relationships in high-density docosylsilane bonded stationary phases by Raman spectroscopy and comparison to octadecylsilane bonded stationary phases, Anal. Chem. 78 (2006) 5813–5822, https://doi.org/10.1021/ac060385p.
[36] L. Slavov, M.V. Abrashev, T. Merodiiska, C. Gelev, R.E. Vandenberghe, I. Markova-Deneva, I. Nedkov, Raman spectroscopy investigation of magnetite nanoparticles in ferrofluids, J. Magn. Magn. Mater. 322 (2010) 1904–1911, https://doi.org/10.1016/j.jmmm.2010.01.005.
[37] A.M. Jubb, H.C. Allen, Vibrational spectroscopic characterization of hematite, maghemite, and magnetite thin films produced by vapor deposition, ACS Appl. Mater. Interfaces. 2 (2010) 2804–2812, https://doi.org/10.1021/am1004943.
[38] O.N. Shebanova, P. Lazor, Raman spectroscopic study of magnetite ($FeFe_2O_4$): a new assignment for the vibrational spectrum, J. Solid State Chem. 174 (2003) 424–430, https://doi.org/10.1016/S0022-4596(03)00294-9.
[39] F. Montagne, O. Mondain-Monval, C. Pichot, H. Mozzanega, A. Elaissari, Preparation and characterization of narrow sized (o/w) magnetic emulsion, J. Magn. Magn. Mater. 250 (2002) 302–312, https://doi.org/10.1016/S0304-8853(02)00412-2.
[40] K. Yang, H. Peng, Y. Wen, N. Li, Re-examination of characteristic FTIR spectrum of secondary layer in bilayer oleic acid-coated Fe_3O_4 nanoparticles, Appl. Surf. Sci. 256 (2010) 3093–3097, https://doi.org/10.1016/j.apsusc.2009.11.079.
[41] I.A. Bakhteeva, I.V. Medvedeva, M.A. Uimin, I.V. Byzov, S.V. Zhakov, A.E. Yermakov, N.N. Shchegoleva, Magnetic sedimentation and aggregation of Fe_3O_4@SiO_2 nanoparticles in water medium, Sep. Purif. Technol. 159 (2016) 35–42, https://doi.org/10.1016/j.seppur.2015.12.043.
[42] S. Ayyappan, G. Gnanaprakash, G. Panneerselvam, M.P. Antony, J. Philip, Effect of surfactant monolayer on reduction of Fe_3O_4 nanoparticles under vacuum, J. Phys. Chem. C. 112 (2008) 18376–18383, https://doi.org/10.1021/jp8052899.
[43] L. Khanna, N.K. Verma, Silica/potassium ferrite nanocomposite: Structural, morphological, magnetic, thermal and in vitro cytotoxicity analysis, Mater. Sci. Eng. B. 178 (2013) 1230–1239, https://doi.org/10.1016/j.mseb.2013.08.004.
[44] L. You, Z. Wu, T. Kim, K. Lee, Kinetics and thermodynamics of bromophenol blue adsorption by a mesoporous hybrid gel derived from tetraethoxysilane and bis (trimethoxysilyl)hexane, J. Colloid Interface Sci. 300 (2006) 526–535, https://doi.org/10.1016/j.jcis.2006.04.039.
[45] A. Kumar, M. Petrič, B. Kričej, J. Žigon, J. Tywoniak, P. Hajek, A.S. Škapin, M. Pavlič, Liquefied-wood-based polyurethane–nanosilica hybrid coatings and hydrophobization by self-assembled monolayers of orthotrichlorosilane (OTS), ACS Sustain. Chem. Eng. 3 (2015) 2533–2541, https://doi.org/10.1021/acssuschemeng.5b00723.
[46] J. Ballarre, I. Manjubala, W.H. Schreiner, J.C. Orellano, P. Fratzl, S. Ceré, Improving the osteointegration and bone–implant interface by incorporation of bioactive particles in sol–gel coatings of stainless steel implants, Acta Biomater. 6 (2010) 1601–1609, https://doi.org/10.1016/j.actbio.2009.10.015.
[47] L.L. Vatta, R.D. Sanderson, K.R. Koch, An investigation into the potential large-scale continuous magnetite nanoparticle synthesis by high-pressure impinging stream reactors, J. Magn. Magn. Mater. 311 (2007) 114–119, https://doi.org/10.1016/j.jmmm.2006.10.1199.
[48] M.S. Dababneh, N.Y. Ayoub, I. Odeh, N.M. Laham, Viscosity, resistivity and surface tension measurements of Fe_3O_4 ferrofluid, J. Magn. Magn. Mater. 125 (1993) 34–38, https://doi.org/10.1016/0304-8853(93)90815-J.
[49] S. Tanvir, L. Qiao, Surface tension of nanofluid-type fuels containing suspended nanomaterials, Nanoscale Res. Lett. 7 (2012) 226, https://doi.org/10.1186/1556-276X-7-226.
[50] G.M. Ritcey, Solvent Extraction: Principles and Applications to Process Metallurgy, second ed., G.M. Ritcey & Associates Inc., Hong Kong, 2006.
[51] A.S. Guimarães, P.S. da Silva, M.B. Mansur, Purification of nickel from multi-component aqueous sulfuric solutions by synergistic solvent extraction using Cyanex 272 and Versatic 10, Hydrometallurgy 150 (2014) 173–177, https://doi.org/10.1016/j.hydromet.2014.10.005.
[52] M.B. Mansur, M.J. Slater, E.C. Biscaia Jr, Reactive extraction of zinc sulfate with bis (2-ethylhexyl)phosphoric acid in a short Kühni column used in batch mode, Ind. Eng. Chem. Res. 42 (2003) 4068–4076, https://doi.org/10.1021/ie020883y.
[53] A.M. Atta, A.O. Ezzat, A.I. Hashem, Synthesis and application of monodisperse hydrophobic magnetite nanoparticles as an oil spill collector using an ionic liquid, RSC Adv. 7 (2017) 16524–16530, https://doi.org/10.1039/C7RA02426F.